Hindawi
Advances in Materials Science and Engineering
Volume 2022, Article ID 1466501, 13 pages
https://doi.org/10.1155/2022/1466501

Research Article

Experimental Analysis of Recycled Aggregate Concrete Beams and Correction Formulas for the Crack Resistance Calculation

Xuyong Chen,[1,2] Zhixin Zhang,[1] Zhifeng Xu,[1,2] Qiaoyun Wu,[1,2] Jianping Fan,[3] and Xuri Zhao[4]

[1]*School of Civil Engineering and Architecture, Wuhan Institute of Technology, Wuhan 430073, Hubei, China*
[2]*Hubei Provincial Engineering Research Center for Green Civil Engineering Materials and Structures, Wuhan 430073, Hubei, China*
[3]*School of Civil and Hydraulic Engineering, Huazhong University of Science and Technology, Wuhan, Wuhan 430073, Hubei, China*
[4]*China Construction Commercial Concrete Co. Ltd, Wuhan 430073, Hubei, China*

Correspondence should be addressed to Zhifeng Xu; 20120102@wit.edu.cn

Received 11 January 2022; Accepted 12 March 2022; Published 29 March 2022

Academic Editor: Dora Foti

This paper studies the similarities and the differences between natural aggregate concrete (NAC) beams and recycled aggregate concrete (RAC) beams in terms of concrete material properties, bearing capacity, and crack resistance and further proposes correction formulas for cracking moment calculation of RAC beams that consider different recycled aggregate substitution ratios. First, the basic mechanical properties (e.g., cube compressive strength, axial compressive strength, and elastic modulus) of RAC blocks were tested; second, comparative bending tests of RAC beams and natural aggregate concrete beams were conducted, in order to obtain the cracking moments, yield bending moments, ultimate bending moments, mid-span deflections and crack development forms; finally, numerical simulations were performed to investigate the cracking performances of RAC beams. Through analyzing the experimental results, it is found that the crack development pattern of RAC beams resembles that of natural aggregate concrete beams, while the cracking performance of RAC beams significantly deviates from that of NAC beams. Finally, the correction formulas for the cracking moment calculation of RAC beams are proposed based on the numerical simulation results and verified by data from other researchers, which can be regarded as a correction for the cracking moment calculation formulas in the current code for RAC beams with respect to varied recycled concrete aggregate substitution ratios.

1. Introduction

With the developments of urbanization and advancements of infrastructure constructions, concrete, as the most common engineering material in constructions, is now experiencing a soar in its consumption. At the same time, exploitations of tremendous nonrenewable resources and generations of a large amount of construction wastes are consequently unavoidable, which is, however, against the global concept of environmental protections and sustainable developments [1]. Therefore, many scholars have recently focused on recycled aggregate concrete (RAC) and its components [2–4]. Nevertheless, before actual engineering applications, it is necessary to comprehensively evaluate the strength, stiffness, stability, and other indicators of RAC members, in order to make the designs and the manufacturing to be consistent. As the most crucial mechanical property, the bearing capacity of RAC beams has been extensively studied [5, 6]. Many studies show that the bending strength of RAC beams is similar to that of natural aggregate concrete (NAC) beams, in which the substitution ratio of recycled concrete aggregates (NCA) has little effect on the bending strength [7–9]. Yet, some researchers believe that when the substitution ratio of NCA is less than 50%, the bending strength of RAC beams is almost the same as that of NAC beams; while when the substitution ratio reaches 100%,

the bending strength of RAC beams can decrease significantly [10]. As for the bending stiffness, the mainstream viewpoint states that the influence of recycled aggregate substitution ratio on mid-span deflection is much higher than that of reinforcement ratio [7, 8, 11, 12], which is still true for the case when natural fine aggregate (NFC) is replaced by recycled fine aggregate [13, 14]. On the other hand, to promote the applications of components made of RAC, the serviceability limit states should also be taken into account, in which the crack resistance is of paramount importance. The cracking behavior of concrete beams is basically determined by the maximum tensile strain. Some researchers demonstrate that, with the increase of substitution ratio of NCA, the maximum tensile strain of RAC beams goes higher than that of NAC beams, resulting in poor tensile properties and increasing ductility [15]. When the substitution ratio of NCA hits 100%, the cracking moment of RAC beams decreases to a value about 25% lower than that of NAC beams, causing a loss of stiffness, premature cracking, and early withdrawal from the working stage [16, 17]. In addition, the crack width and crack spacing should also be considered, which is affected by the bond-slipping behavior between concrete and reinforcement [9, 18]. Although the fact that the decrease of stiffness after cracking leads to the decrease of its bond strength is doubtless, there are few quantitative studies on the influence of recycled aggregate substitution ratio on the crack development.

From the above discussion, it can be concluded that existing researches on the mechanical properties of RAC members lack of quantitative analysis, which is insufficient for practical engineering. To this end, taking the bending performance of RAC beams as the research subject, this paper studies the influence of replacement ratio and longitudinal reinforcement ratio on the bending performance of RAC beams, whose conclusions provide practical structural designs with useful guidance. In order to analyze the short-term bending behaviors, four-point bending tests were carried out on full-scale RAC beams. The cracking moment, yield moment, ultimate moment, and mid-span deflection are measured and analyzed, in which the cracking moment is analyzed in detail. The experimental results were analyzed by two stages: the first stage aims to understand the influence of NCA and longitudinal tensile reinforcement ratio on the mechanical properties of RAC beams, and four kinds of test beams with varied recycled aggregate substitution ratios and three different reinforcement ratios were designed manufactured and tested, whose test results were compared and analyzed; in the second stage, the practicability of the cracking moment formulas in the current code for RAC beams is analyzed, which compared the relative error between the test values and the corresponding values computed by the code. The results show that RAC beams and NAC beams share similar crack development patterns, while their cracking performances deviate from each other significantly. Thus, the current code cannot accurately describe the cracking behaviors of recycled aggregate concrete beams, which requires corrections. Hence, correction formulas for the cracking moment calculation with respect to RAC beams are proposed and verified based on a series of numerical analyses and experimental data from different researchers.

This paper is organized as follows: Section 2 describes the test method and the test content; in Section 3, the test results are presented and analyzed in detail, and the similarities and differences between RAC beams and NAC beams are obtained; the correction formulas for the cracking moment calculation of RAC beams are proposed and verified in Section 4.

2. Experimental Tests of RAC Beams

This section presents the details of the experimental tests of RAC beams in terms of material properties, specimen configurations, and experimental schemes.

2.1. Material Properties. The cement used in this test was Huaxin brand pm42.5 ordinary Portland cement, and the reducing ratio of water reducing agent was 15%. The natural aggregate (NA) used in the test was nature crushed stone, and the aggregate was the continuous gradation meeting the standard JGJ 52–2006 [19]. RCA consists of three kinds of coarse aggregates with different particle sizes, which were mixed into a continuous gradation of 5–25 mm that satisfying the classification standard of class II aggregates in GB/T 25177–2010 [20]. The fine aggregates used in the test were all natural fine aggregates, and the fineness modulus is medium coarse. The physical properties of various aggregates are shown in Table 1.

For C30 concrete defined by JGJ55-2011 [21], the water-cement ratio is 0.49, and the substitution ratios of NCA are 0% (reference group), 50%, 70%, and 100%, respectively. The corresponding four kinds of numbers were, respectively, NAC, RAC-50, RAC-70, and RAC-100. It can be seen from Table 1 that the water absorption of NCA is dramatically higher than that of natural aggregates, which is caused by the adhesion of mortar on the surface of NCA [22]. This characteristic leads to greater free water absorption of NCA in the mixing process of concrete, while the decrease of W/C value contributes to the decrease of the cohesion of RAC. To solve this problem, additional water was added. The mix proportion parameters are shown in Table 2 and additional water consumption is shown in Table 3. The reinforcements in the beam body meet the relevant provisions of GB/T 50010–2010 [23]. The stirrups and erecting reinforcements were HPB335 with a diameter of 8 mm, and the tensile reinforcements were HRB400. According to the requirements for reinforcement ratio, 14 mm, 16 mm, and 18 mm are used, respectively. In order to obtain the mechanical parameters (shown in Table 4), the tensile test of stressed reinforcement is carried out using the tensile test method of reinforcement according to GB/T 28900–2012 [24].

2.2. Specimen Configurations. A total of 7 beams were designed and manufactured in this study, with a cross-sectional size of 150 mm × 300 mm and a length of 1800 mm. The variables considered are substitution ratio of NCA and reinforcement ratio of longitudinal stressed reinforcements,

Table 1: Physical properties of aggregates.

Aggregate type	Particle size range (mm)	Apparent density (kg/m^3)	Water absorption (%)	Water absorption and mud content (%)	Crushing index	Fineness modulus
NFA	≤5	2559	2.2	1.2	-	2.8
NA	5–20	2673	0.6	0.9	11	—
RCA	5–20	2534	4.6	0.2	17	—

Table 2: Concrete consumption per unit volume.

Label	Substitution ratio of RCA (%)	W/C	Material consumption (kg/m3)				
			Cement	Sand	NA	RCA	Water reducing agent
NAC	0	0.49	367.4	686.5	1167.2	0	4.04
RAC-50	50				583.6	553.3	
RAC-70	70				350.2	774.6	
RAC-100	100				0	1106.6	

Table 3: Additional water consumption per unit volume.

Category of coarse aggregate	Label	Water absorption (%)	Substitution ratio (%)	Additional water consumption (kg)
NA	NAC	0.6	0	0
RCA	RAC-50	4.6	50	23.34
	RAC-70		70	32.68
	RAC-100		100	46.69

Table 4: Mechanical properties of stressed reinforcement.

Diameter of reinforcement (mm)	Yield strength (MPa)	Ultimate strength (MPa)	Elastic modulus (GPa)
14	455	627	205
16	466	635	203
18	432	607	200

which is divided into the following two groups: Group 1 has 5 beams with varied substitution ratio of NCA, the stressed reinforcements were 2C14, the substitution ratios of NCA are, respectively, 0%, 30%, 50%, 70%, and 100%, and the numbers were NAC-0.77, RAC-30-0.77, RAC-50-0.77, RAC-70-0.77, and RAC-100-0.77 respectively; Group 2 has 3 beams with varied reinforcement ratios. The substitution ratios of NCA were all 100%, the load-bearing steel bars were 2 HRB400 14, 2 HRB400 16, and 2 HRB400 18; the reinforcement ratios were 0.77%, 1.01%, and 1.28%; and the numbers were, namely, RAC-100-0.77, RAC-100-1.01, and RAC-100-1.28. In order to reduce the influence of stirrups on the mechanical analysis of the pure bending section, neither stirrup nor erection bar was arranged at the pure bending section at the middle of the span. The specific design parameters of the test beam are shown in Table 5, and the details of reinforcements are shown in Figure 1. The test beam was poured and maintained in the Structure and Disassembly Laboratory of Wuhan University of Technology, and the test beams of two sizes (100 mm × 100 mm × 100 mm and 100 mm × 100 mm × 300 mm respectively) were reserved for 28 days under the same conditions (shown in Figure 2).

2.3. Experimental Schemes. The loading mode of the test beams was four-point bending. The main instruments were the reaction frame and the 500 kN electro-hydraulic servo brake, and then, the load was evenly distributed through the distribution beam. The bending beam was simply supported by a roller and a pin support both placing at 150 mm away from each end of the beam, respectively. The distribution beam was also supported on the test beam by a roller and a pin support that were both placed at 650 mm away from each end of the beam, respectively (shown in Figure 3). The loading procedure was strictly in accordance with GB/T 50152–2012 [25]. In order to facilitate the observation and analysis of the crack development pattern, a small square of 100 mm × 100 mm was marked in front and at the back of the beam. Before the formal loading, the preloading was carried out 2 times in order to check whether the dial gauge, strain gauge, and mechanical sensor can work normally. In the formal loading stage, when the loading force value was close to 80% of the cracking load, yield load, and ultimate load, the load value of each level should not exceed 5% of their corresponding calculated values, and the stable load time should be controlled at least 10 minutes to observe the development trend of mechanical properties.

The deflections at the middle of the span and the strain of the tensile reinforcement in the beam were measured by dial indicator and DH3818 y, respectively. The six strain gauges were symmetrically arranged on the tensile steel bars on both sides of the pure bending section at the middle of the span, and the dial indicator was arranged at the bottom of the middle of the span, as shown in Figure 3.

Table 5: Design parameters of test beams.

Specimen number	Cross section (mm×mm)	Length (mm)	Tensile reinforcement	Erecting reinforcement	Stirrup	Reinforcement ratio (%)	Thickness of protective layer (mm)
NAC-0.77	150×300	1800	2 HRB400 14	HPB300 8	HPB300@100	0.77	20
RAC-30-0.77			2 HRB400 14			0.77	
RAC-50-0.77			2 HRB400 14			0.77	
RAC-70-0.77			2 HRB400 14			0.77	
RAC-100-0.77			2 HRB400 14			0.77	
RAC-100-1.01			2 HRB400 16			1.01	
RAC-100-1.28			2 HRB400 18			1.28	

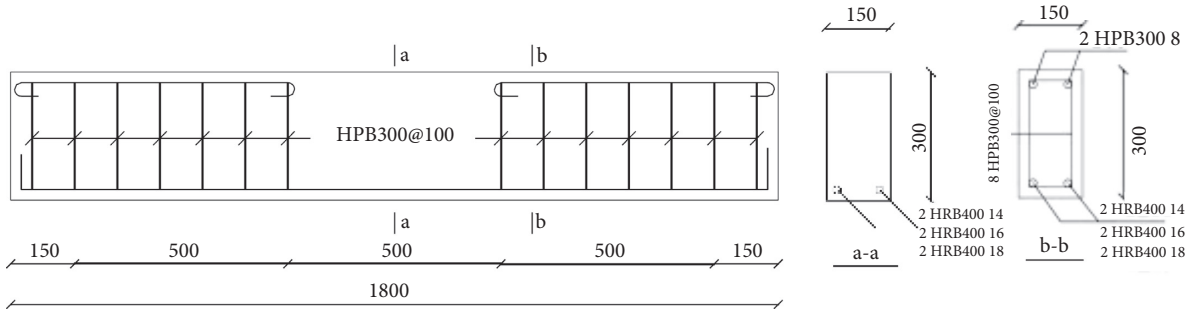

Figure 1: Reinforcement details of test beams (mm).

(a) (b)

Figure 2: Experimental specimens. (a) Curing test block under the same condition. (b) Casting and forming.

3. Test Results and Discussions

In this section, the test results are presented and investigated, and the similarities and differences between RAC beams and NAC beams are studied.

3.1. Material Properties of RAC. In order to obtain the material properties of RAC, blocks of RAC with varied recycled aggregate substitution ratios were manufactured and tested according to GB/T 50080–2016 and GB/T 50081–2019 [26, 27]. The slump index was used to characterize its workability. The data show that, when additional water is considered, even with an increased substitution ratio of NCA, the slump will not decrease significantly, whose slump can still meet the standard of flowing concrete. On the mechanical properties of the indicators, the cube compressive strength, axial compressive strength, and elastic modulus are mainly measured. The test results are shown in Table 6, from which it can be seen that the three mechanical properties decrease with the increase of substitution ratio of NCA. The main reason for this phenomenon is that there are two different interface transition zones (ITZ): one is the interface between new and old cement mortar, and the other is the interface between new cement mortar and recycled aggregate. This ITZ weakens bonds between aggregate and cement, reducing the strength of concrete and increasing its deformation performance [28].

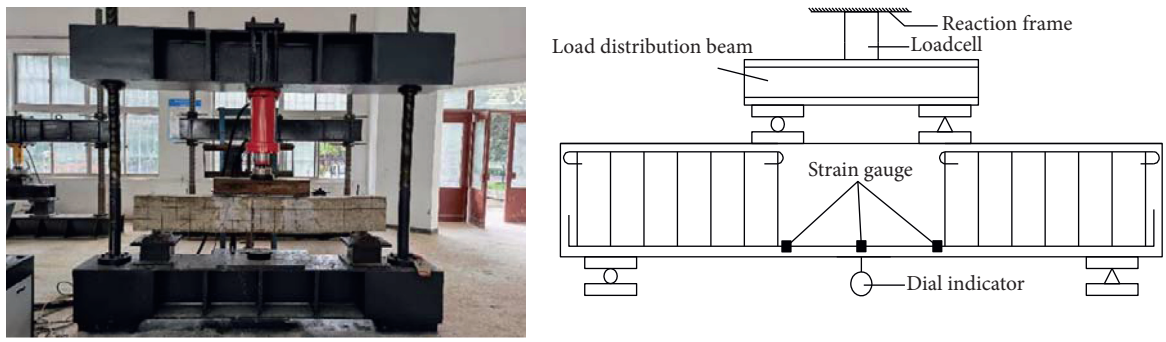

Figure 3: Loading mode and layout of measuring instruments. (a) Test device and loading mode. (b) Layout of strain gauge and displacement gauge.

Table 6: Physical and mechanical properties of concrete.

Substitution ratio of RCA (%)	Slump (mm)	f_{cu} (MPa)	f_c (MPa)	E_c (GPa)
0	144	35.4	28.7	41.3
50	138	34.7	28.5	38.7
70	140	32.1	27.6	32.2
100	141	30.3	27.3	30.8

3.2. Analysis of Bearing Capacity of RAC Beams. The test results show that the test beams with different replacement ratios of recycled aggregate and different reinforcement ratios can meet the ductility design, which means the stressed reinforcement yields before the beam failure. Simultaneously, due to the existence of the pure bending section at the mid-span, the bending cracks first appeared at the bottom of both ends of the pure bending section. As the load increases, the number and length of cracks increase gradually. When there were inclined cracks in the shear-bending section, the number of cracks at the middle of the span tended to be stable. When the load reached the yielding load, the width of the mid-span crack became wider, the crack length developed longer, and the mid-span deflection started to increase rapidly. Finally, the concrete at the mid-span was crushed, and the test beam was damaged (shown in Figure 4).

Figure 4: Failure state of the test beam.

The load-mid-span deflection curves of each test beam are shown in Figure 5, from which it can be seen that the stress development trend of the RAC beam and NAC beam is similar. This indicates that the structural engineering application of RAC is feasible. The development stage of the beams is divided into the elastic stage, the working stage with cracks, and the failure stage. It can be seen from the figure that the substitution ratio of NCA has little effect on the ultimate load of the RAC beams compared to the significant effect due to the reinforcement ratio. This phenomenon is the same as that of NAC beams. In addition, similar to the NAC beam, it can be seen from Figure 5 that, with the increase of reinforcement ratio, the mid-span deflection of steel bars at the yielding stage increases gradually, but the deflection increments decrease.

By recording the cracking moment(M_{cr}^t), yielding moment(M_y), and ultimate moment(M_u), the bending performances of RAC beams with different recycled aggregate replacement ratios and different reinforcement ratios were compared, whose results are shown in Table 7. The bending moment values in the table are all obtained through the conversion of test load values. It can be seen from Table 7 that with the increase of the substitution ratio of NCA, the cracking moment decreases significantly, indicating that RAC has lower tensile strengths that lead to premature cracking of RAC beams. At this junction, it should be pointed out that the maximum reduction of the cracking moment can reach 31.9%. On the other hand, the change of recycled aggregate substitution ratio has little effect on the yield moment and ultimate moment, which is due to the ductility design (with appropriate reinforcement ratio) of concrete beams. In contrast, the reinforcement ratio has a great influence on the yield moment and ultimate moment, whose influence on the cracking moment is negligible though.

Figure 6 shows the load-strain curves of the loading steel, which demonstrates that all the steel bars reach the yield point before the failure of the beam, and therefore, RAC beams meet the ductile failure characteristics. The use of tensile reinforcements also increases the yield limit and the

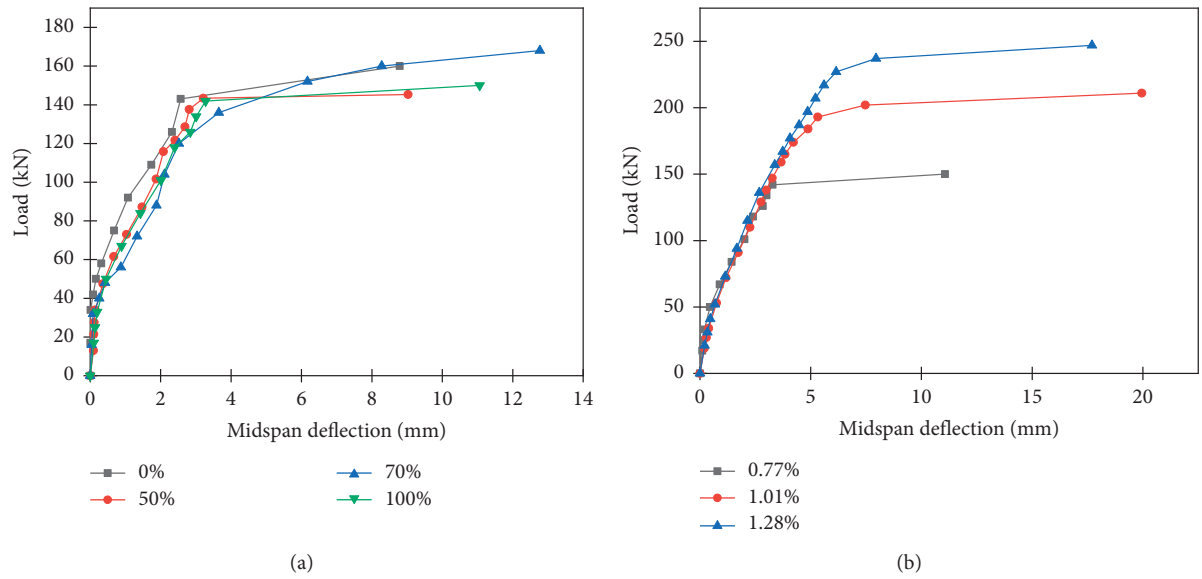

Figure 5: Load-mid-span deflection curves. (a) Substitution ratio of RCA. (b) Reinforcement ratio of tensile reinforcement.

Table 7: Mechanical properties of test beams.

Test beam number	M_{cr}^{t} $(kN \cdot m)$	M_{y} $(kN \cdot m)$	M_{u} $(kN \cdot m)$	M_{cr}^{t}/M_{u} (%)
NC–0.77	10.5	35.75	40	26.25
RAC50–0.77	7.53	35.25	39.25	19.59
RAC70–0.77	6.59	36	40	17.88
RAC100–0.77	7.2	35.5	38.5	18.83
RAC100–1.01	7.25	46	51.5	14.56
RAC100–1.28	7.13	56.75	60.5	11.79

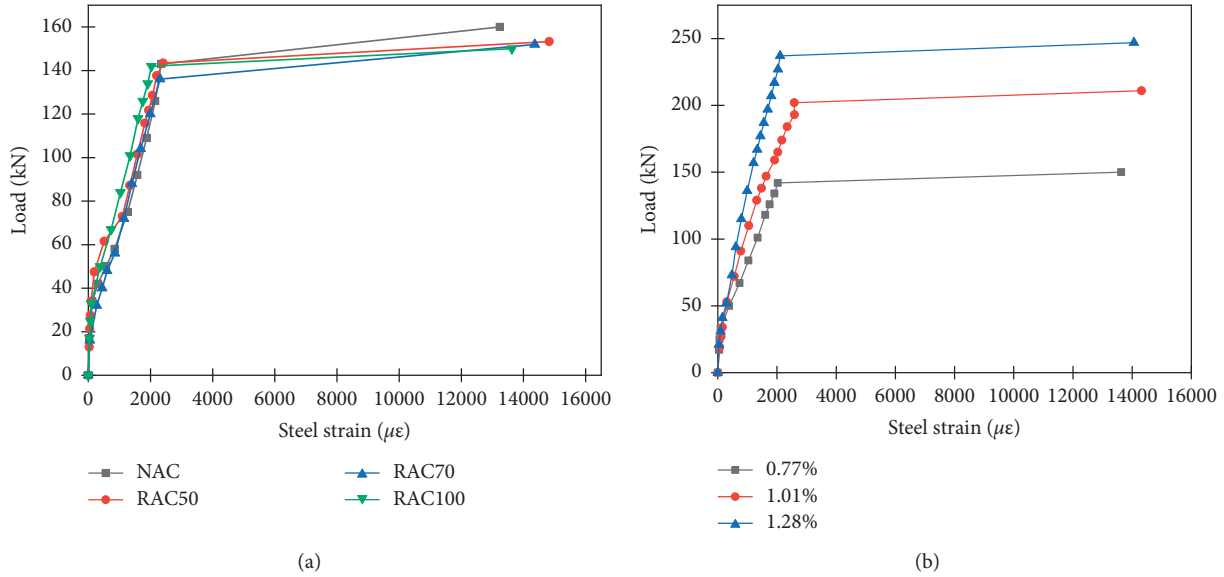

Figure 6: Load VS steel strain curves. (a) Substitution ratio of RCA. (b) Reinforcement ratio of tensile reinforcements.

ultimate strength of beams, which weakens the role of concrete in the experimental failure of simply supported beams. Therefore, the change of substitution ratio of NCA has no effect on the yield limit or the ultimate strength, and there is no obvious difference among the ultimate state between the RAC beam and NAC beam. This conclusion is inconsistent with the research results of Knaack and other scholars [7–9].

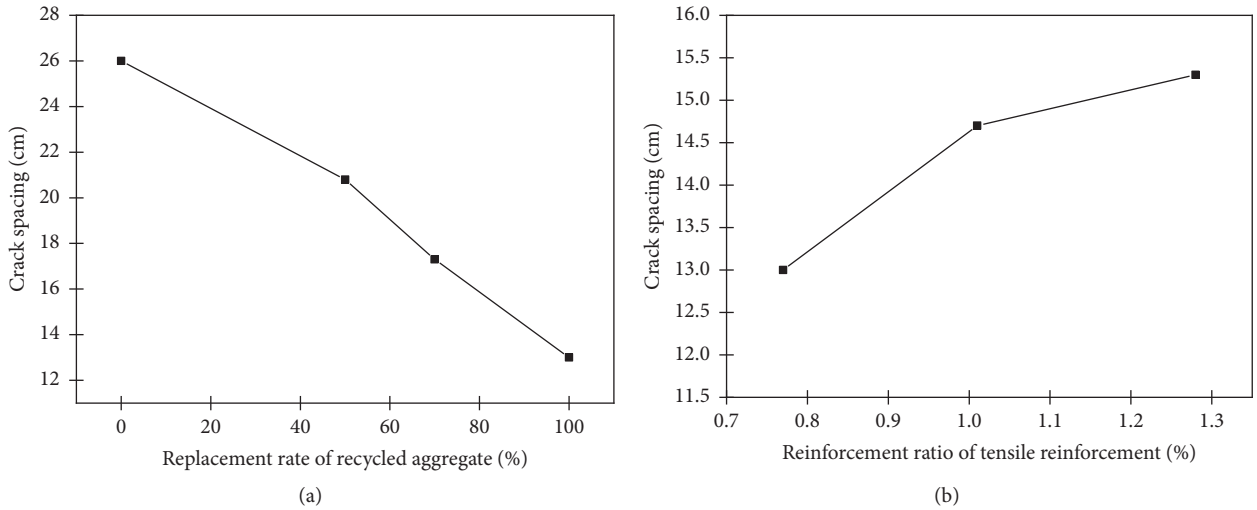

Figure 7: Crack development diagram of test beams. (a) NAC-0.77. (b) RAC-50-0.77. (c) RAC-70-0.77. (d) RAC-100-0.77. (e) RAC-100-1.01. (f) RAC-100-1.28.

3.3. Crack Resistance of RAC Beams. Crack resistance is an important index for the serviceability limit state of concrete members. In order to analyze the crack resistance of RAC beams, the ratio of cracking moment to ultimate moment was calculated (M_{cr}^{t}/M_u) (as shown in Table 7). It is obvious that RAC beams will crack earlier than natural concrete beams under the same reinforcement ratio. In the experiment, the NAC beam cracked when the applied bending moment reached about 25% of the ultimate bending moment, while for the RAC beam, it will crack when the applied bending moment is only 17% to 19% of the ultimate bending moment.

Figure 7 is the crack development diagram of each test beam, from which it can be seen that the test beams with different substitution ratios all have similar crack development patterns. The crack of all test beams started from the pure bending section near the load application point, whose length was less than 50 mm. As the load increases, the length and the number of cracks increase gradually, while the change of crack width was inconspicuous. When the load increases to a certain threshold, oblique shear cracks appear on both sides of the beam, while there is nearly no crack in the supporting area. When the longitudinal reinforcement yields, the mid-span deflection suddenly increased, and the vertical cracks became wider than 1.7 mm, showing the failure of the beam.

It can be seen from Figure 8 that, under the same reinforcement ratio, as the substitution ratio of NCA increases, the crack number in the mid-span increases gradually, and the crack spacing decreases gradually. This is because, although the bond effect between RAC and reinforcement decreases and the crack spacing increases, the reduction of elastic modulus and tensile strength of RAC trigger the beams easier to crack, which reduces the crack spacing. However, even if the substitution ratio of NCA remains unchanged and the reinforcement ratio increases, the crack spacing also increases, which is in line with the development law of NAC.

4. Correction Formulas for the Cracking Moment Calculation of RAC Beams

The correction formulas for the cracking moment calculation of RAC beams are proposed and verified in this section, which can account for different RCA substitution ratios.

4.1. Theoretical Analysis of Cracking Moment Calculation of RAC Beams. According to the above discussion, the crack resistance of RAC beams is mainly affected by the ultimate tensile strain of RAC. Some studies stated that the tensile peak strain of RAC is greater than that of ordinary concrete [29]. Wu et al. demonstrated that the ultimate strain of RAC is similar to that of NAC [30]. And he further assumed that, when the substitution ratio of recycled aggregate is 100%, the ultimate tensile strain of the RAC beam is 1.5 times the peak strain, which is 2 times of that NAC. Hence, the stress-strain diagram of normal section of RAC beam when cracking can be obtained is shown in Figure 9.

The balance equation of horizontal force is established as follows (shown in Figure 9):

$$\frac{1}{2}bx\frac{x}{h-x}\frac{3}{2}f_t^R = \frac{2}{3}b(h-x)f_t^R. \tag{1}$$

The height of the compression zone is calculated as $x = 0.485h$. And the maximum compressive stress is 1.413 f_t^R.

The cracking moment of the RAC beam is calculated as follows:

$$M_{cr}^R = 1.338W_0 f_t^R, \tag{2}$$

where W_0 is the moment of resistance of the section, and for rectangular section, $W_0 = bh^2/6$, and f_t^R is the tensile strength of RAC.

From equation (2), it can be seen that the basic value of plastic influence coefficient of resistance moment (γ_m^R) of RAC beam is 1.338, which is less than the standard value of

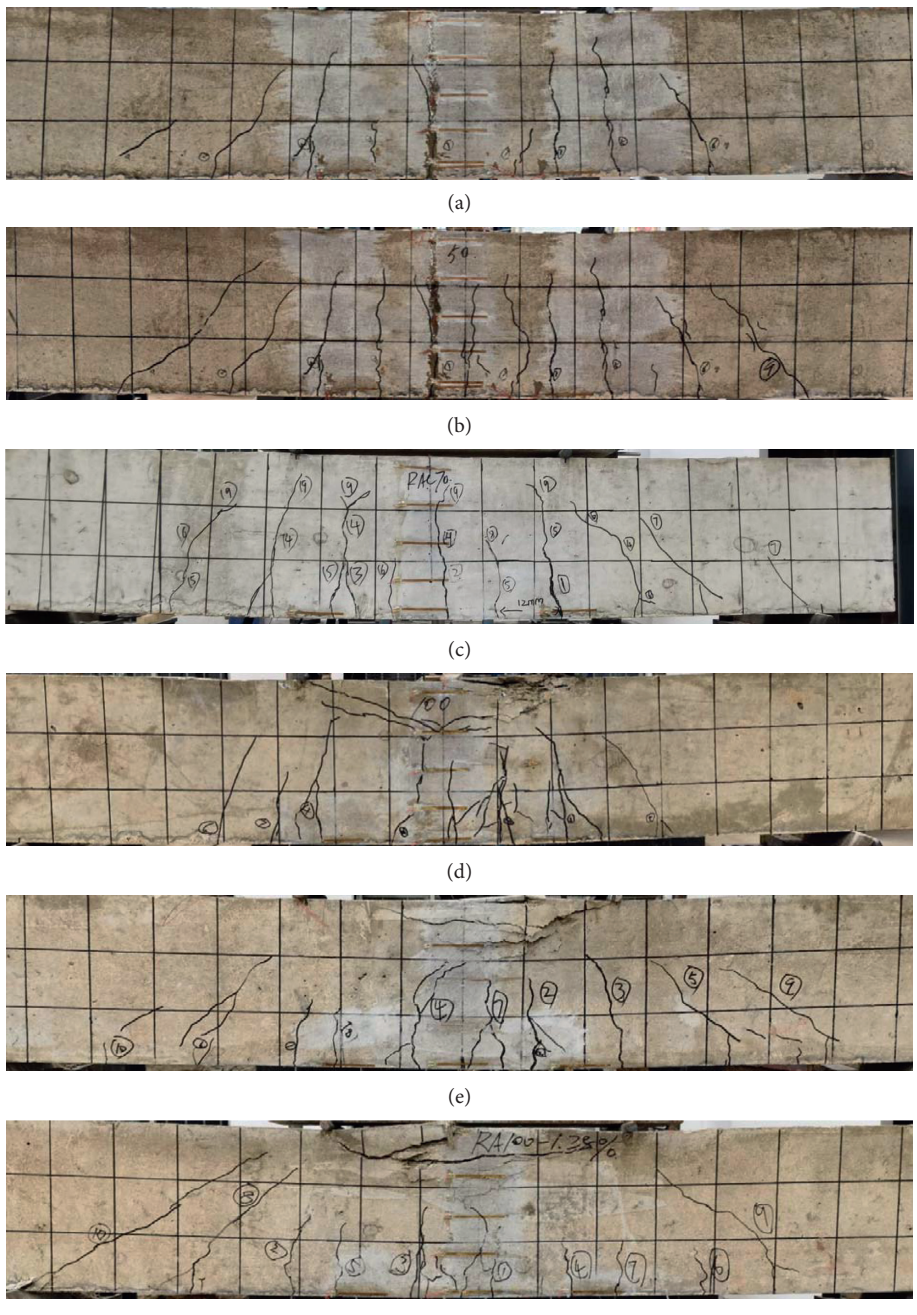

(a)

(b)

(c)

(d)

(e)

(f)

Figure 8: Variations of crack spacing of RAC beams. (a) Substitution ratio of RCA. (b) Reinforcement ratio of tensile reinforcements.

NAC 1.55 [23]. In other words, when the tensile peak strain increases and the ultimate tensile strain remains unchanged, the crack resistance of RAC beams will inevitably decrease. Since the cracking strain of RAC in this paper is assumed and the influence of reinforcement is not considered, it is necessary to further verify the calculation formulas of the cracking moment.

4.2. Correction Formulas for the Cracking Moment Calculation Based on Numerical Simulations. In order to obtain the cracking moment of RAC beams with respect to different substitution ratios of recycled aggregate, a three-dimensional finite element model was established and analyzed by ABAQUS software based on the existing test data.

4.2.1. Geometry, Material Modeling, and Meshing of the Finite Element Simulations. As shown in Figure 10, the corresponding finite element model of the test beams is presented. Figure 10(a) shows the concrete beam geometry, the load location, and the support arrangement. Figure 10(b) shows the geometry of the steel skeleton model. The reinforcement ratio of all the models was 0.77% without

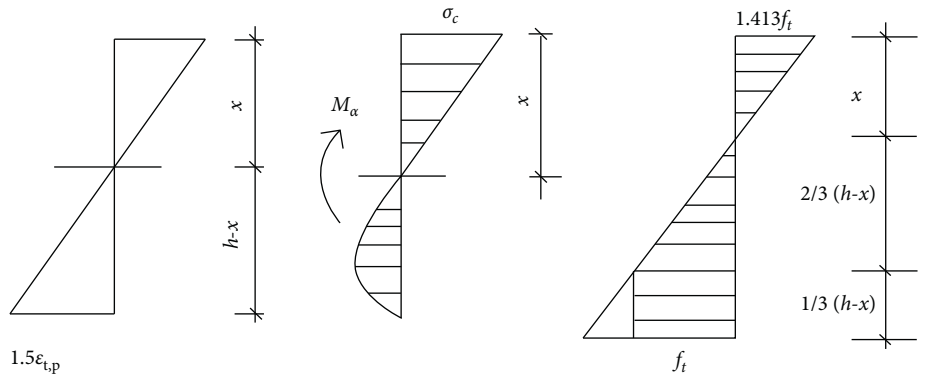

Figure 9: Stress-strain relationship of RAC beams.

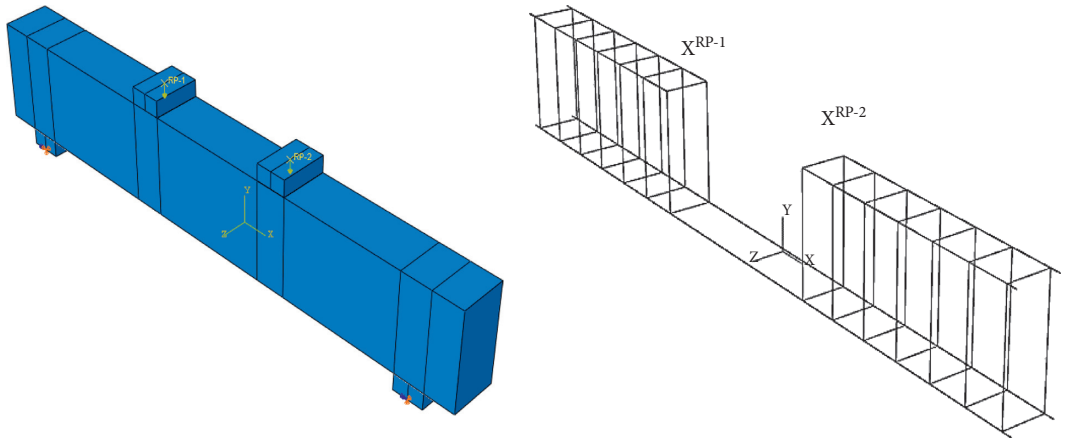

(a) (b)

Figure 10: Finite element model of the simply supported RAC beam. (a) Beam model. (b) Steel skeleton model.

considering the change of reinforcement ratio in the numerical analysis. The concrete damage plastic model (CDP) was used to define the constitutive characteristics of the beam. The constitutive curve of RAC proposed by Ding has a good fit with that of NAC, which can avoid the attenuation of elastic modulus of concrete in the elastic stage [31]. Therefore, such a constitutive curve is adopted in the simulation, which is described by equation (3) [31].

$$y = \begin{cases} \dfrac{A_{n(r)}x + \left(B_{n(r)} - 1\right)x^2}{1 + \left(A_{n(r)} - 2\right)x + B_{n(r)}x^2} & x \le 1 \\ \dfrac{x}{\alpha_{n(r)}(x-1)^2 + x} & x > 1 \end{cases}, \tag{3}$$

where $A_{n(r)}$ is the ratio of elastic modulus to peak secant modulus of RAC; $B_{n(r)}$ is the parameter of ascending section; $\alpha_{n(r)}$ is the parameter of descending section; $y = \sigma/f_c$ (σ is the stress, f_c is the test value of axial compressive strength); $x = \varepsilon/\varepsilon_c$ (ε is the strain, ε_c is the peak strain). When RAC is under uniaxial compression ($n = 1$), equation (3) can be rewritten as follows:

$$\begin{aligned} A_{1(r)} &= \frac{(1-0.3r)(1+0.2r)}{1-0.1r} \times 9.1 f_{cu}^{-4/9}, \\ B_{1(r)} &= \frac{5\left(A_{1(r)} - 1\right)^2}{3}, \\ \alpha_{1(r)} &= 2.5 \times 10^{-5} f_{cu}^3. \end{aligned} \tag{4}$$

When the RAC is in a uniaxial tension state and ($n = 2$), then equation (3) become

$$\begin{aligned} A_{2(r)} &= 1.306 \frac{(1-0.3r)(1+0.1r)}{1-0.1r}, \\ B_{2(r)} &= \frac{5\left(A_{2(r)} - 1\right)^2}{3}, \\ \alpha_{2(r)} &= 1 + 3f_{cu}^2 + 10^{-4}, \end{aligned} \tag{5}$$

where r is the substitution ratio of RCA, and f_{cu} is the test value of concrete cube compressive strength.

In order to obtain the damage parameter of the damage constitutive formula in the CDP model, this paper adopts the calculation formula derived from Sidoroff's energy equivalence principle, whose specific formula is as follows [32]:

$$\delta = E_0 (1 - d)^2 \varepsilon. \quad (6)$$

The following calculation formula of damage factor is obtained after conversion:

$$d = 1 - \sqrt{\frac{\delta}{E_0 \varepsilon}}, \quad (7)$$

where E_0 is the initial elastic modulus; d is the damage factor. In order to obtain the basic parameters of the damage constitutive model and match the basic mechanical data of the test beam, the basic mechanical property tests corresponding to the test beam are carried out. The specific data are shown in Table 8.

In the model, a three-dimensional solid element with 8 nodes and 6 facets using reduced integral (C3D8R) was used to define the main concrete element. The reinforcement skeleton element consists of longitudinal reinforcement, vertical reinforcement, and stirrup, which was simulated by a three-dimensional two-node truss element (T3D2). The T3D2 element only has three degrees of freedom and can only undertake axial tension or pressure, which was suitable to simulate the components with large stiffness. The cushion block unit was simulated by the C3D8R element. In order to increase the accuracy, the mesh size of the main beam was set to 10 mm, while the length of the reinforcement skeleton was 25 mm.

4.2.2. Boundary Conditions and Loading Configurations. The boundary conditions refer to the constraint of the simply supported beam in the actual situation, and cushion blocks were placed at 150 mm (lower edge) and 650 mm from both ends of the beam. Three axial constraints and rotation constraints around Y axis and Z axis were set on the cushion block in the opposite direction of X axis. Axial constraints in Y and Z directions and rotation constraints around Y axis and Z axis were set on the cushion block in the positive direction of X axis. In order to simulate the actual loading system, the loading mode of monotonic concentrated force was used. The load of the two loading points was 100 kN (200 kN in total). The bond-slip behavior between steel and concrete was simulated by the built-in region constraint of the finite element node, which can simulate the ideal slip state between steel and concrete.

4.2.3. Analysis of the Numerical Simulation Results. It can be seen from Figure 6 that, when the concrete in the tensile zone of the lower part of the beam cracks, the tensile stress is borne by the reinforcement, which will cause the strain mutation of the reinforcement. Therefore, the inflection point of the bending moment steel strain curve obtained by ABAQUS postprocessing can be used as the sign for the cracking bending moment (M_{cr}^c). In order to compare the simulation value of the cracking bending moment with the corresponding result calculated from the current code value, the cracking moment formula (8) in GB/T 50010–2010 is used for calculation [23]. The numerical simulation results and results calculated by the code are shown in Table 9.

$$M_{cr} = \gamma f_{tk} W_0, \quad (8)$$

$$\gamma = \gamma_m \left(0.7 + \frac{120}{h}\right), \quad (9)$$

where M_{cr} is the cracking moment; f_{tk} is the axial tensile strength; W_0 is the elastic moment of resistance after conversion of cross section; γ is the plastic influence coefficient of section resistance moment; γ_m is the basic value of the plastic influence coefficient of the resistance moment of the section, which is 1.55 for rectangular sections.

It can be seen from Table 9 that, with the increase of substitution ratio of recycled aggregate, the relative error between the code calculation value and the test value increases obviously. That is, the calculation formula of cracking moment for NAC beam is no longer applicable to RAC beam. The ratio of the cracking moment test value (M_{cr}^c) to the code calculation value (M_{cr}) is taken as y value (see Table 9), and the substitution ratio of recycled aggregate is taken as r for curving fitting (Figure 11). Consequently, the correction formula (10) of the basic value of the plastic influence coefficient of the corresponding section moment of resistance can be obtained by curve fitting, whose correlation coefficient $R^2 = 0.992$.

$$y = 0.772 + 0.215 \times e^{-x/0.643}. \quad (10)$$

The modified basic value of plastic influence coefficient of section moment of resistance and the calculated value of cracking moment are as follows:

$$\gamma_m^R = y \times \gamma_m,$$
$$\gamma^R = \gamma_m^R \left(0.7 + \frac{120}{h}\right), \quad (11)$$

$$M_{cr}^R = \gamma^R f_{tk} W_0, \quad (12)$$

where γ_m^R, γ^R, and M_{cr}^R are the basic value of the plastic influence coefficient of section moment of resistance, the plastic influence coefficient of section moment of resistance, and the value of cracking moment, respectively.

4.3. Verification of Correction Formulas for the Cracking Moment Calculation. In order to verify the proposed modified formula (12) for cracking moment of RAC beams proposed, this section analyzes the test data obtained from other researchers and further compares the test results with the calculation results of (12). The results are shown in Table 10, from which it can be seen that the calculation results obtained by the modified formulas are in good agreement with the experimental data obtained by various researchers. The average relative error is 3.83%, the standard deviation of relative error is 2.12%, and the maximum absolute relative error is 7.66%, which further proves the correctness and the accuracy of (12).

Table 8: Basic test parameters.

Aggregate type	Specimen number	f_{cu}/MPa	f_c/MPa	E_c/GPa
NC	NAC	37.1	29.7	41.6
		36	28.6	41.4
		33.2	27.1	41.2
RAC	RAC-30	37.5	30.5	35.4
		35.8	29	33.7
		35.5	27.7	32.1
	RAC-50	34.9	29.1	30.8
		34.7	28.6	30.1
		34.5	28.3	31
	RAC-70	32.9	28.2	30.9
		32.2	27.5	30.4
		31.2	27.3	30.2
	RAC-100	30.9	29.4	28.5
		30.3	27.5	27
		29.6	26.3	26.3

Table 9: Numerical simulation results of cracking moment.

Aggregate type	Beam number	M_{cr}^{c} (kN·m)	M_{cr} (kN·m)	Relative error	M_{cr}^{c}/M_{cr}
NC	NC-1	10.781	11.348	0.053	0.950
	NC-2	10.493	10.93	0.042	0.960
	NC-3	11.541	11.722	0.016	0.985
RAC	RAC-50-1	8.732	10.211	0.169	0.855
	RAC-50-2	8.44	9.905	0.174	0.852
	RAC-50-3	8.154	9.470	0.161	0.861
	RAC-70-1	8.344	9.840	0.179	0.848
	RAC-70-2	7.577	9.001	0.188	0.842
	RAC-70-3	7.186	8.581	0.194	0.837
	RAC-100-1	7.578	9.348	0.234	0.811
	RAC-100-2	6.675	8.361	0.253	0.798
	RAC-100-3	6.846	8.594	0.255	0.797

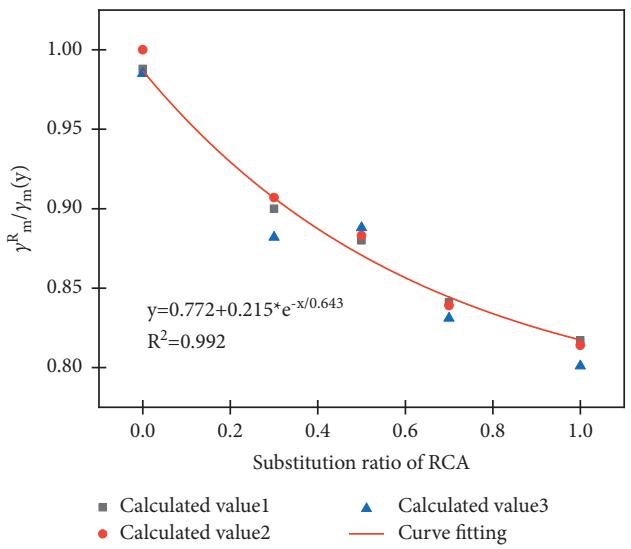

Figure 11: Fitting curve.

Table 10: Verification of the proposed formulas.

Researchers	Maximum relative error (%)	r (%)	M_{cr}^{R} (kN·m)	M_{cr}^{t} (kN·m)	M_{cr}^{t}/M_{cr}^{R}
This study	20	50	7.42	7.53	1.03
		70	6.68	6.59	0.99
		100	7.04	7.2	1.02
Wang [33]	25	30	8.35	8.99	1.08
				8.6	1.03
		50	8.34	8.38	1.00
				8.65	1.04
		70	7.76	7.45	0.96
				7.38	0.95
		100	7.65	7.35	0.96
				7.45	0.97
Lan [34]	20	50	8	7.5	0.94
		100	7.21	7.5	1.04
Du [35]	24	50	21.85	20.3	0.93
		70	20.86	21.75	1.04
Mean value					0.997

5. Conclusions

This paper first studies the similarities and the differences between NAC beams and RAC beams with respect to concrete material properties, bearing capacity, and crack resistance via experimental observations and tests. Based on the experimental test results, correction formulas for the cracking moment calculation of RAC beams are proposed and verified through numerical simulations and optimal fitting of test data from other researchers. Moreover, the following conclusions are drawn:

(1) Under the same reinforcement ratio, the cracking moment of RAC beams decreases as the substitution ratio of RCA increases, while the substitution ratio of RCA has an only subtle influence on the yield moment or the ultimate moment of RAC beams due to the ductile design

(2) The reinforcement ratio has the same effect on the yield performance and the ultimate bearing capacity of both RAC beams and NAC beams

(3) The premature cracking effect increases with an increasing substitution ratio of RCA

(4) Although the cracking behavior of RAC beams is similar to that of natural aggregate concrete beams, the decrease of bond effect between recycled aggregate concrete and reinforcement will lead to an increase of crack width, while the decreases of elastic modulus and tensile strength of recycled aggregate concrete both lead to early cracking, the decrease of crack spacing, increasing reinforcement strain, and the increase of midspan deflection

(5) It is found that the cracking moment of RAC beams gradually decreases as the substitution ratio increases, in which the cracking moment of RAC beams can be more than 25% lower than that of NAC beams if RCA completely replaces the natural aggregates, indicating the current code is not applicable to RAC beams on cracking moment calculation

(6) The corrected formulas of the cracking moment calculation have sufficient accuracy, whose average relative error is merely 3.83%.

Data Availability

The data used to support the findings of this study are included within the article.

Conflicts of Interest

The authors declare that they have no conflicts of interest regarding the publication of this article.

Acknowledgments

The authors wish to acknowledge the financial support provided by the National Natural Science Foundation of China (No. 52178301), the Key Research and Development Program of Hubei Science and Technology Department (No. 2020BAB071), and the Science Research Foundation of Wuhan Institute of Technology (K2021030).

References

[1] A. Kanellopoulos, P. Savva, M. F. Petrou, I. Ioannou, and S. Pantazopoulou, "Assessing the quality of concrete - reinforcement interface in Self Compacting Concrete," *Construction and Building Materials*, vol. 240, Article ID 117933, 2020.

[2] D. Foti and D. Cavallo, "Mechanical behavior of concretes made with non-conventional organic origin calcareous aggregates," *Construction and Building Materials*, vol. 179, pp. 100–106, 2018.

[3] D. Foti and M. Lerna, "New mortar mixes with chemically depolymerized waste PET aggregates," *Advances in Materials Science and Engineering*, vol. 2020, Article ID 8424936, 9 pages, 2020.

[4] D. Foti, M. Lerna, M. Sabbà, and V. Vacca, "Mechanical characteristics and water absorption properties of blast-furnace slag concretes with fly ashes or microsilica additions," *Applied Sciences*, vol. 9, no. 7, p. 1279, 2019.

[5] B. Lei, H. Wu, Y. S. Yan, and C. H. Rao, "Research on the calculation method for bending rigidity of recycled concrete beams," *Advanced Materials Research*, vol. 919–921, pp. 1396–1399, 2014.

[6] Y. Gui-xin, W. Jin, and Y. Qiang, "Study on deflection of recycled concrete beams," *Engineering Mechanics*, vol. 28, no. 2, pp. 147–151, 2011.

[7] A. M. Knaack and Y. C. Kurama, "Behavior of reinforced concrete beams with recycled concrete coarse aggregates," *Journal of Structural Engineering*, vol. 141, no. 3, Article ID B4014009, 2015.

[8] M. Arezoumandi, A. Smith, J. S. Volz, and K. H. Khayat, "An experimental study on flexural strength of reinforced concrete beams with 100% recycled concrete aggregate," *Engineering Structures*, vol. 88, pp. 154–162, 2015.

[9] S. Seara-Paz, B. González-Fonteboa, F. Martínez-Abella, and J. Eiras-López, "Flexural performance of reinforced concrete beams made with recycled concrete coarse aggregate," *Engineering Structures*, vol. 156, pp. 32–45, 2018.

[10] R. Dhir, M. Limbachiya, T. Leelawat, and B. Bs, "Suitability OF recycled concrete aggregate for use IN BS 5328 designated mixes," *Proceedings of the Institution of Civil Engineers-Structures and buildings*, vol. 134, no. 3, pp. 257–274, 1999.

[11] I. S. Ignjatović, S. B. Marinković, Z. M. Mišković, and A. R. Savić, "Flexural behavior of reinforced recycled aggregate concrete beams under short-term loading," *Materials and Structures*, vol. 46, no. 6, pp. 1045–1059, 2013.

[12] F. Yu, C. B. Yin, and M. Jiang, "Study on the recycled concrete beam's stiffness," *Applied Mechanics and Materials*, vol. 193-194, pp. 1361–1364, 2012.

[13] L. Evangelista and J. De Brito, "Flexural behaviour of reinforced concrete beams made with fine recycled concrete aggregates," *KSCE Journal of civil engineering*, vol. 21, no. 1, pp. 353–363, 2017.

[14] W.-C. Choi, H.-D. Yun, and S.-W. Kim, "Flexural performance of reinforced recycled aggregate concrete beams," *Magazine of Concrete Research*, vol. 64, no. 9, pp. 837–848, 2012.

[15] J. S. Ryu, "An experimental study on the effect of recycled aggregate on concrete properties," *Magazine of Concrete Research*, vol. 54, no. 1, pp. 7–12, 2002.

[16] Q. Yu, M. Shi, Y. Cheng, M. Wang, and H.-z. Chen, "Fe3O4@Au/polyaniline multifunctional nanocomposites: their preparation and optical, electrical and magnetic properties," *Nanotechnology*, vol. 19, no. 26, Article ID 265702, 2008.

[17] G. Kaklauskas, V. Gribniak, D. Bacinskas, and P. Vainiunas, "Shrinkage influence on tension stiffening in concrete members," *Engineering Structures*, vol. 31, no. 6, pp. 1305–1312, 2009.

[18] Z. Deng, Y. Wang, H. Yang, and J. Qian, "Research on crack behavior of recycled concrete beams under short-term loading," *KSCE Journal of Civil Engineering*, vol. 22, no. 5, pp. 1763–1770, 2018.

[19] Jgj-52, *Standard for Technical Requirements and Test Method of Sand and Crushed Stone (Or Gravel) for Ordinary concrete*, China Architecture& Building Press, Beijing, China, 2006.

[20] Gb/T-25177, *Recycled Coarse Aggregate for concrete*, China Standards Press, Beijing, China, 2010.

[21] Jgj-55, *Recycled Coarse Aggregate for concrete*, China Construction Industry Press, Beijing, China, 2011.

[22] M. Joseph, L. Boehme, Z. Sierens, and L. Vandewalle, "Water absorption variability of recycled concrete aggregates," *Magazine of Concrete Research*, vol. 67, no. 11, pp. 592–597, 2015.

[23] Gb/T-50010, *Code for Design of concrete Structures*, China Construction Industry Press, Beijing, China, 2010.

[24] GB/T-28900, *Test Methods of Steel for Reinforcement of concrete*, China Standards Press, Beijing, China, 2012.

[25] GB/T-50152, *Standard for Test Method of concrete Structures*, China Construction Industry Press, Beijing, China, 2012.

[26] Gb/T-50080, *Standard for Test Methods of Performance on Ordinary Fresh concrete*, China Construction Industry Press, Beijing, China, 2016.

[27] Gb/T-50081, *Standard for Test Methods of concrete Physical and Mechanical Properties*, China Construction Industry Press, Beijing, China, 2019.

[28] S. Seara-Paz, V. Corinaldesi, B. González-Fonteboa, and F. Martínez-Abella, "Influence of recycled coarse aggregates characteristics on mechanical properties of structural concrete," *European Journal of Environmental and Civil Engineering*, vol. 20, no. sup1, pp. s123–s139, 2016.

[29] J.-z. Xiao and J.-b. Li, "Study on relationships between strength indexes of recycled concrete," *Journal of Building Materials*, vol. 2, 2005.

[30] J. Wu, D.-f. Ding, and W. Zhang, "Experimental study on shear behavior of recycled aggregate concrete beams," *Journal of Hohai University (Natural Sciences)*, vol. 1, 2010.

[31] F.-x. Ding, C.-j. Fang, Y.-z. Gong, Z.-w. Yu, and L.-n. Hu, "Unified calculation method of uniaxial mechanical performance index of recycled concrete," *Journal of Architecture and Civil Engineering*, vol. 4, 2014.

[32] L. Tian and J. Hou, "Reasonable plastic damaged factor of concrete damaged plastic model of ABAQUS," *Journal of Hubei University (Natural Science)*, vol. 37, no. 4, pp. 340–345, 2015.

[33] J. Wang and C. Zhang, "Experimental study on flexural behavior of recycled concrete beams," *Journal of Lanzhou University of Technology*, vol. 42, no. 2, pp. 130–134, 2016.

[34] Y. Lan, *Experimental study on flexural behavior of recycled concrete beams*, Journal of Tongji University, Shang Hai, China, 2004.

[35] Z. H. Du, T. Hao, and L. X. Liu, "Experimental study on flexural property of reinforced concrete beams with recycled aggregate of construction waste," *Key Engineering Materials*, vol. 517, pp. 601–605, 2012.